Global compilation of interferometric synthetic aperture radar earthquake source models:
2. Effects of 3-D Earth structure

A. M. G. Ferreira,[1,2] J. Weston,[1] and G. J. Funning[3]

[1]   We carry out long-period surface wave centroid moment tensor (CMT) inversions using various global tomographic models and two different forward modeling techniques for 32 large earthquakes previously studied using interferometric synthetic aperture radar (InSAR) data. Since InSAR methods provide an alternative and independent way of locating and characterizing shallow continental earthquakes, comparisons of our source parameters with those from InSAR are a novel way to assess limitations in the InSAR models as well as the effects of inaccurate wave propagation formulations and/or 3-D Earth structure on earthquake source determinations. We show that comparing InSAR results with our seismic solutions is valuable to identify inaccuracies in the earthquake slip distribution retrieved using InSAR. Moreover, we find that using more accurate formulations, together with the best fitting Earth models, substantially reduces biases and differences between moment magnitude and fault strike determined using InSAR and seismic data. As expected for long-period surface wave source inversions for shallow earthquakes, the fault dip and rake angles are difficult to constrain, but we show that when using the best fitting Earth models, differences to InSAR estimates are reduced. Moreover, spurious deviations from a pure double-couple earthquake mechanism are on average smaller for the best fitting Earth models and the more accurate formulation of wave propagation. There are large differences between InSAR epicentral locations and those obtained in this study and, on average, no clear improvements to the Global CMT locations are achieved. This suggests that higher-resolution Earth models are necessary to further refine long-period CMT epicentral locations.

1.   Introduction

[2]   Accurate earthquake point source parameters (spatio-temporal location, seismic moment and focal mechanism) provide key first-order information for detailed studies of the earthquake source process. Moreover, they are an important input to our understanding of active tectonics and provide valuable information for improved seismic and tsunami hazard evaluation.

[3]   Of the various methods for the retrieval of earthquake point source models from teleseismic long-period data, the centroid moment tensor (CMT) approach [*Dziewonski et al.*, 1981] is particularly attractive, as it is quick, accurate and provides a simple and concise description of the earthquake source. The CMT procedure uses seismic waveforms in the time domain filtered in an adequate frequency range to determine the earthquake's centroid coordinates (latitude, longitude, depth and origin time) and the seismic moment tensor. The systematic application of the CMT method to global earthquakes led to the global CMT (GCMT) catalog, which is widely used in tectonic studies, in seismic hazard assessment and in a broad range of applications that require the calculation of theoretical seismograms.

[4]   However, various sources of error can affect CMT source parameter determinations. Noteworthy, the use of simplifying assumptions both about Earth structure and seismic wave propagation imposes errors in CMT determinations, particularly for estimates of the centroid epicenter and depth, the origin time [e.g., *Dziewonski and Woodhouse*, 1983; *Hjörleifsdóttir and Ekström*, 2010] and the seismic moment [e.g., *Patton and Randall*, 2002]. Despite recent progress in seismic tomography that led to the production of a variety of global tomographic models, most earthquake source studies use spherically symmetric Earth models to simulate seismic wave propagation, as the modeling is relatively simple and computationally efficient. The effects of

[1]School of Environmental Sciences, University of East Anglia, Norwich, UK.
[2]Also at ICIST, Instituto Superior Técnico, Technical University of Lisbon, Lisbon, Portugal.
[3]Department of Earth Sciences, University of California, Riverside, California, USA.

lateral heterogeneity on the data are then often taken into account either empirically or by using approximate theoretical corrections. The former approach consists, e.g., of aligning the calculated waveforms with the observations, assuming that the corresponding phase differences are only due to propagation effects [e.g., *Bernardi et al.*, 2004]. The latter approach includes the use of approximations such as the classical great circle approximation (GCA), which assumes that phase corrections are given in terms of mean phase slowness along the source-receiver great circle, and which neglects the effects of heterogeneity on seismic amplitudes [e.g., *Woodhouse and Dziewonski*, 1984; *Pondrelli et al.*, 2002]. While applying empirical corrections may lead to a loss of information about the earthquake source process, approximate corrections such as the GCA exclude important effects of three-dimensional structure on the data, such as focusing and defocusing effects and changes in source excitation due to local structures. These effects affect mainly the amplitudes of seismic waves [e.g., *Ferreira and Woodhouse*, 2007a], which play an important role, e.g., when estimating the seismic moment of an earthquake.

[5] In order to address these issues, *Ferreira and Woodhouse* [2006] investigated the errors in long-period CMT determinations by implementing a centroid technique for the rapid determination of earthquake source parameters using both the GCA and a more complete, full formulation of surface wave ray theory. Moreover, they used four different 3-D Earth models. This work showed that more accurate modeling of Earth structure helps to constrain the seismic moment tensor. In addition, when applying their technique to real earthquakes, it was shown that using four different Earth models yields a large range of earthquake source solutions that explain the data equally well. This highlighted the nonuniqueness and uncertainties in CMT solutions. However, a detailed evaluation of the quality of the retrieved earthquake source parameters was not possible, due to the lack of objective, independent, benchmark solutions for the earthquakes studied. Indeed, the general nonexistence of independent solutions makes the assessment of earthquake source models quite challenging.

[6] Ongoing efforts in satellite geodesy techniques can help us tackling these issues, as they provide an alternative and independent way of characterizing earthquakes. For example, progress in Interferometric Synthetic Aperture Radar (InSAR) methods has enabled the investigation of over 50 global continental earthquakes, which were compiled into an archive of InSAR centroid moment tensor (ICMT) source parameters in the companion study by *Weston et al.* [2011] (hereafter referred to as paper 1). Such archive constitutes a new opportunity to examine errors in both seismic and InSAR models of earthquakes and in particular to assess uncertainties arising from simplifying assumptions about both seismic wave propagation and the structure of the Earth's interior.

[7] In this study, we use, for the first time, information independent of seismology to validate the choice of Earth model and of forward modeling for CMT inversions. We exploit this by applying the CMT method of *Ferreira and Woodhouse* [2006] to 32 large shallow continental earthquakes that are included in the ICMT archive. We start by analyzing in detail the various solutions obtained for two illustrative earthquakes occurring in distinct tectonic settings and compare them with ICMT parameters. We then show the overall results for all the earthquakes studied. We analyze the impact of using different theoretical approaches and Earth models on the seismic source inversions and benchmark them against InSAR solutions.

2. Method and Data

[8] In this study we focus on large earthquakes ($M_w \geq$ 6.5), for which teleseismic waveforms recorded by the Global Seismic Network are well above the noise level. Specifically, we use the method of *Ferreira and Woodhouse* [2006] to carry out long-period surface wave source inversions for 32 large ($M_w \geq 6.5$) earthquakes that have been studied previously using InSAR data and that are included in the ICMT database compiled in paper 1. The earthquakes that we study have occurred between 1992 and 2005 and are shallower than 60 km (see Figure 1 for the geographical location and Table 1 for a list of the earthquakes studied). Of the 32 earthquakes used, 17 are strike-slip earthquakes, 12 have thrust and 3 have normal fault mechanisms.

[9] We calculate synthetic seismograms and partial derivatives with respect to the six elements of the seismic moment tensor and the four space-time coordinates of the centroid location using two different theories: (1) the classical great circle approximation (GCA) [e.g., *Woodhouse and Dziewonski*, 1984], which corrects 1-D Earth synthetic seismograms for lateral heterogeneity through the use of first-order path-averaged phase corrections, and (2) full ray theory (FRT), which combines the concept of local normal modes with exact ray tracing as a function of frequency. According to FRT, the seismic wavefield involves a source, a propagation and a receiver term. The source term takes into account the wave's excitation based upon the local earth structure at the source as well as deviations in the takeoff azimuth. The propagation term accounts for path deviations from the source-receiver great circle and focusing and defocusing effects on the waves' amplitudes due to lateral heterogeneity. Finally, the receiver term includes the effect of the local earth structure at the receiver's location. For more details about the full ray theory and its numerical implementation, see *Ferreira and Woodhouse* [2007b].

Figure 1. Geographical location of the earthquakes (white stars) and comparison of the phase velocity perturbation maps for fundamental mode Rayleigh waves with period $T = 150$ s used in this study (these are also called mantle waves, with a maximum of sensitivity at depths of around 300 km). (a) S20RTS denotes a map calculated from mantle model S20RTS combined with CRUST2.0, as explained in section 2. The other maps are published results (b) by *van Heijst and Woodhouse* [1999] (vHW99), (c) by *Trampert and Woodhouse* [1995] (TW95) and (d) by *Trampert and Woodhouse* [1996] (TW96). Phase velocities are relative to PREM. The map of vHW99 is expanded up to harmonic degree $l = 40$ and has the greatest amount of short-wavelength structure. We expand the S20RTS maps only up to harmonic degree $l = 20$, because S20RTS is a degree 20 model. TW95 and TW96 are both expanded up to harmonic degree $l = 40$, but for higher degrees, TW96 has shorter scale structure.
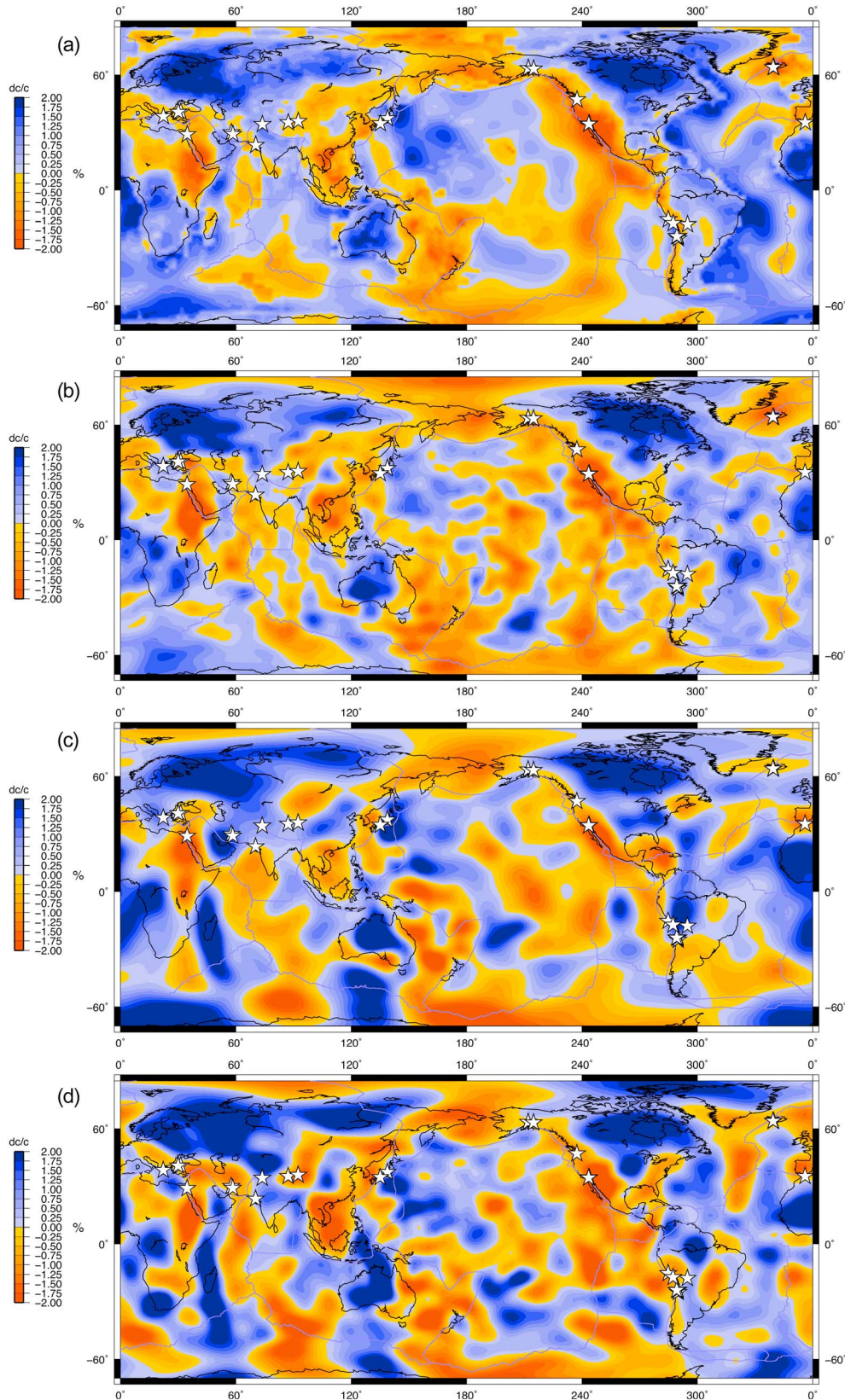
Figure 1

Table 1. Earthquakes Used in This Study That Have Been Studied Previously Using InSAR Data and Corresponding Moment Magnitudes[a]

Event	Date	Location	M_w
1	22.05.98	Aiquile, Bolivia	6.5
2	19.04.96	northern Chile	6.7
3	11.07.93	northern Chile	6.8
4	30.01.98	northern Chile	7.1
5	12.11.96	Nazca Ridge, Peru	7.7
6	13.06.05	Tarapaca, Chile	7.8
7	30.07.95	Antofagasta, Chile	8.1
8	23.06.01	Arequipa, Peru	8.5
9	15.06.95	Aigion, Greece	6.3
10	14.03.98	Fandoqa, Iran	6.6
11	26.12.03	Bam, Iran	6.6
12	13.05.95	Kozani-Grevena, Greece	6.5
13	22.11.95	Nuweiba, Egypt	7.1
14	12.11.99	Duzce, Turkey	7.1
15	17.08.99	Izmit, Turkey	7.5
16	24.02.04	Al Hoceima, Morocco	6.5
17	21.05.03	Zemmouri, Algeria	6.8
18	08.11.97	Manyi, Tibet	7.4
19	26.01.01	Bhuj, India	7.5
20	08.10.05	Kashmir	7.6
21	14.11.01	Kokoxili, Tibet	7.8
22	20.03.05	Fukuoka, Japan	6.5
23	24.10.04	Niigata, Japan	6.8
24	16.01.95	Kobe, Japan	7.2
25	17.06.00	Iceland	6.5
26	21.06.00	Iceland	6.4
27	23.10.02	Nenana Mt., Alaska	6.7
28	03.11.02	Denali, Alaska	7.9
29	17.01.94	Northridge	6.6
30	28.02.01	Nisqually	6.8
31	16.10.99	Hector Mine	7.2
32	28.06.92	Landers	7.3

[a]Other ICMT source parameters for these earthquakes are reported by *Weston et al.* [2011]. The earthquakes are ranked according to their geographical location. Dates format is day.month.year (dd.mm.yy).

[10] In this study, calculations of the source and receiver terms are always carried out using the crustal model CRUST2.0 [*Bassin et al.*, 2000] combined with the mantle model S20RTS [*Ritsema et al.*, 1999]. In order to compute the propagation term, we use phase velocity maps that we calculated from the model S20RTS combined with CRUST2.0 expanded up to harmonic degree $l_{max} = 20$ (lateral spatial resolution of about 2000 km at the Earth's surface). We refer to the combination of these phase velocity maps with the 3-D model used for source and receiver calculations as the S20RTS model. Moreover, we also calculate the propagation term using the degree 40 dispersion maps of *van Heijst and Woodhouse* [1999] and *Trampert and Woodhouse* [1995, 1996]. We shall refer to the combination of 3-D mantle model used for source and receiver calculations with these dispersion maps as vHW99, TW95 and TW96, respectively (see Figure 1). Among the latter phase velocity distributions, the maps of *van Heijst and Woodhouse* [1999] generally contain the shortest scale structure, followed by those produced by *Trampert and Woodhouse* [1996]. *Ferreira and Woodhouse* [2007b] showed that the models S20RTS and vHW99 led to the best fit to long-period surface wave data for a different global set of earthquakes to that used in this study. Nevertheless, the data fit differences between these models and TW95 and TW96 were small and as such their significance was not entirely clear.

[11] We minimize differences between theoretical and observed seismograms using an iterative, least squares inversion scheme. We use three-component fundamental mode minor arc surface wave data from the IRIS/IDA global network, which are deconvolved for displacement and convolved with the response of an SRO instrument and low-pass cosine tapered between 135 and 150 s. We use only source-receiver pairs with epicentral distance between 40° and 140° to minimize near-field effects, caustics and multiple-orbit interfering wave trains. The station coverage is fairly uniform in azimuth for all the events and in order to ensure a well-balanced coverage, whenever data from several stations are available in a 5° azimuthal interval, we use only the one with the best signal-to-noise ratio. We verify that for earthquakes occurring in the same region the station coverage is as similar as possible, in order to make the corresponding solutions more comparable.

[12] As in the GCMT technique, we consider a triangular source time function of half duration T_{half}, which is estimated from the seismic moment using the relationship

$$T_{half} = 1.075 \times 10^{-8} M_0^{\frac{1}{3}}, \tag{1}$$

where the seismic moment M_0 is measured in dyn cm and T_{half} is measured in seconds.

[13] We start by carrying out a linear inversion for the seismic moment tensor, assuming the global CMT source location and origin time as a starting solution, which allows us to obtain the initial estimate of the moment tensor. We then proceed to the iterative inversion for moment tensor and hypocentral coordinates. Once the optimal fitting solution is obtained, the best double-couple solution is calculated from the eigenvalues and eigenvectors of the moment tensor, which allows us to determine the seismic moment, the fault strike, dip and rake and the deviation from a pure double-couple mechanism, $\epsilon = \frac{|\lambda|_{min}}{|\lambda|_{max}}$, where λ are the eigenvalues of the seismic moment tensor.

[14] In section 3 we present a detailed analysis of two illustrative earthquakes occurring in different tectonic settings.

3. Analysis of Two Examples of Earthquakes

3.1. The 22 May 1998, M_w = 6.6, Aiquile, Bolivia Earthquake

[15] The 22 May 1998, M_w = 6.6 strike-slip earthquake in Aiquile, Bolivia, was the first Bolivian earthquake studied using InSAR [*Funning et al.*, 2005]. An accurate epicentral location was obtained for the first time in a region with sparse instrumentation and with limited knowledge of its complex crustal structure. Moreover, using InSAR data, it was also possible to place constraints on the slip distribution and geometry of the fault in which this earthquake occurred.

[16] We use 99 three-component seismograms from 42 stations well distributed in azimuth to carry out source inversions for this earthquake. Figure 2 compares results of this study with the Global CMT solution and with the results of *Funning et al.* [2005] from InSAR modeling. Among the various synthetic seismograms calculated for a laterally varying Earth, TW95 is the worst fitting model. Using TW95 produces an overestimation of the moment magnitude (particularly when using the GCA) and a near vertical

Model	Th.	Lat/Lon (°)	M_w	$\psi/\delta/\lambda$	ϵ (%)	m^2	BB
ICMT		-17.90/-65.16	6.55 or 6.53	7/79/171	–	–	
GCMT		-17.60/-65.20	6.55	6/101/178	6	–	
S20RTS	GCA	-17.78/-65.17	6.59	7/114/168	25	0.16	
	FRT	-17.78/-65.16	6.55	5/104/173	14	0.17	
vHW99	GCA	-17.81/-65.12	6.60	4/96/148	23	0.15	
	FRT	-17.80/-65.12	6.56	5/95/158	18	0.15	
TW95	GCA	-17.89/-64.88	6.81	-37/84/92	42	0.24	
	FRT	-17.87/-64.82	6.68	-29/81/100	41	0.23	
TW96	GCA	-17.81/-65.06	6.69	13/157/195	41	0.21	
	FRT	-17.80/-65.04	6.60	10/118/164	40	0.19	

Figure 2. Source parameters for the 1998 Aiquile earthquake. Lat/Lon are the centroid's latitude and longitude; ψ, δ, λ are the fault plane strike, dip and rake of the best double-couple solution; and ϵ quantifies the deviation from a pure double-couple mechanism, $\epsilon = |\lambda|_{min}/|\lambda|_{max}$, where λ are the eigenvalues of the seismic moment tensor. ICMT contains InSAR solutions by *Funning et al.* [2005], and Global CMT parameters are given. Subsequent inversion results are from this study using different Earth models: S20RTS, vHW99, TW95, TW96 and different theoretical approximations: great circle approximation (GCA) and full ray theory (FRT). We do not show the centroid depth because the GCMT source depth has been fixed to $h = 15$ km and for all of our inversions the source became shallower than 15 km, so that we constrained it to be $h = 15$ km. The average data misfit (m^2, see equation (2)) for each of our solutions is also shown. Note that we adopt a convention such that fault dip values greater than 90° mean that the corresponding fault is dipping in the opposite direction to those with dip smaller than 90°.

dip-slip source mechanism, which is very different from that found by *Funning et al.* [2005] and in the GCMT catalog. It is also interesting that the GCMT and best fitting seismic solutions (S20RTS and vHW99) have main fault planes dipping westward, whereas the ICMT main fault plane is dipping eastward. This might be due to difficulties in constraining the fault dip when using seismic CMT methods (particularly when using surface waves only) and/or due to limitations in the InSAR data, as only one pair of SAR images was available to study this earthquake, which had some incoherences due to vegetation in areas with lower elevation. The centroid epicentral location obtained using TW95 is about 30 km away from that determined by *Funning et al.* [2005] (~29 km using the GCA and ~36 km when using the FRT). The best fitting Earth models (S20RTS and vHW99) lead to focal mechanisms that are in reasonable agreement with both the GCMT and ICMT solutions. Interestingly, using the models S20RTS, vHW99 and TW96, we obtain centroid epicentral locations that are at about 11–17 km from the ICMT location, thus being much closer than the GCMT location, which is ~34 km away from the ICMT location. Figure 3 compares the best fitting uniform slip model of *Funning et al.* [2005] and its centroid location (blue circle) with the GCMT location (black circle), the NEIC, ISC and EHB locations (red, black and green stars, respectively) and with the solutions using the various 3-D Earth models in this study (various colored triangles). It is clear that using S20RTS, vHW99 and TW96,

we obtain locations that are closer to the fault plane of *Funning et al.* [2005] than all other solutions.

[17] We note that the ICMT location agrees with the highest intensity shaking in the event [*Funning et al.*, 2005], so for this earthquake, using the Earth models S20RTS, vHW99 and TW96 leads to a significant improvement in earthquake location compared to those used in the GCMT, NEIC, ISC and EHB procedures.

[18] For all laterally varying Earth calculations, the corresponding solutions have non-double-couple components greater than in the GCMT solution, which are particularly large for the models with the poorest fit to the data (TW95 and TW96). Thus, they must be at least partly due to inaccuracies in the Earth models, as suggested by *Henry et al.* [2002], which, combined with the fact that we use long-period surface waves only, lead to difficulties in constraining the dip-slip components of the moment tensor, which can in turn lead to spurious non-double-couple components. The small non-double-couple component in the GCMT solution is possibly due to the fact that for this earthquake the GCMT procedure used both long-period body and surface waves, which should improve the resolution of the dip-slip components of the moment tensor.

3.2. The 14 November 2001, $M_w = 7.8$ Kokoxili, Tibet, Earthquake

[19] The 14 November 2001, $M_w = 7.8$ Kokoxili earthquake (also known as Kunlun) ruptured over 400 km of the
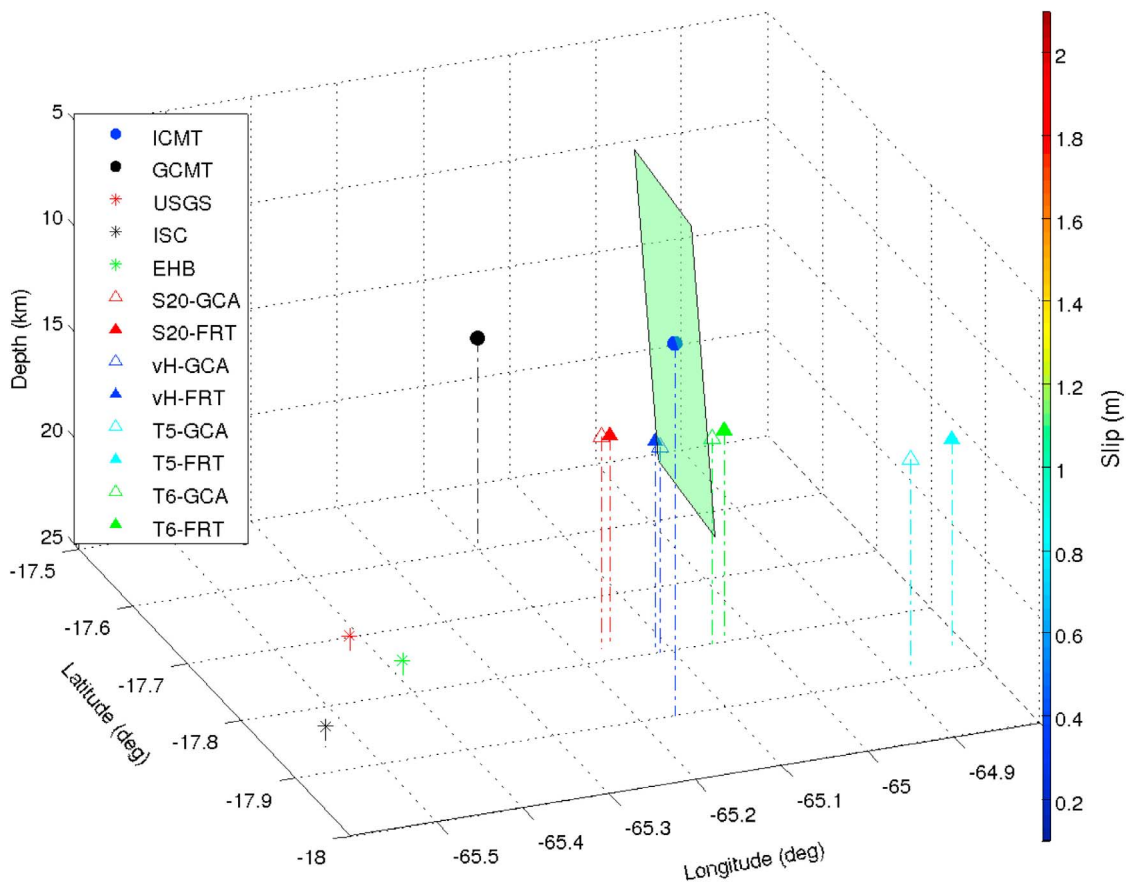
Figure 3. Comparison of centroid locations for the 1998 Aiquile earthquake from various seismic catalogs (GCMT, USGS, ISC and EHB), from our inversions using a variety of Earth models and two different forward modeling strategies (S20-GCA, S20-FRT, vH-GCA, vH-FRT, T5-GCA, T5-FRT, T6-GCA and T6-FRT) and for the centroid obtained by *Funning et al.* [2005] using InSAR data (ICMT). The best fitting uniform slip model of *Funning et al.* [2005] is superimposed on the various centroid locations. S20 denotes the S20RTS model, vH denotes the vHW99 model, T5 denotes the TW95 model and T6 denotes the TW96 model (see text for more details). In order to facilitate the 3-D visualization of the various locations, we also plot vertical dot-dashed lines showing the projection of the various locations to the latitude-longitude plane.

western left-lateral Kunlun fault in northern Tibet, being one of the largest strike-slip events ever recorded. *Lasserre et al.* [2005] studied this earthquake, using InSAR data to estimate the corresponding slip distribution. They found that slip varied substantially along the fault, with six sections of major moment release that correspond to six mapped segments of the Kunlun fault system.

[20] We study this earthquake using 87 seismograms from 40 stations. Figure 4 compares results of this study with the InSAR results by *Lasserre et al.* [2005] and with the Global CMT solution for this earthquake. All laterally varying Earth models fit the data equally well, with a slight deterioration in the misfit when using FRT for TW95 and for TW96. Overall there is good agreement between the various moment magnitudes, with a variability in M_w not exceeding ± 0.1 around the ICMT moment magnitude. The focal mechanisms obtained using the models S20RTS, vHW99 and TW95 agree well with the GCMT focal mechanism, which was determined using only long-period surface waves. Although

the strike and rake of the main fault plane for these solutions agree well with the ICMT solution, there are important differences in the fault dip angle, reaching a maximum difference of 50° for the solution obtained using the S20RTS model (GCA). In order to reduce potential trade-offs in their inversions and given the mechanism of the earthquake, *Lasserre et al.* [2005] decided to model the fault as a vertical surface, i.e., they fixed the fault dip to be 90°. Other studies of this earthquake also found vertical or near-vertical dip fault angles [e.g., *Antolik et al.*, 2004; *Robinson et al.*, 2006]. Thus, the observed differences in fault dip angle must be due to the limitations of long-period surface waves in determining this source parameter. The focal mechanisms for the model TW96 are quite oblique, with rake angles of $\lambda \approx 59°$ and $\lambda \approx 25°$ and thus differ significantly from the other focal mechanisms. Since large, shallow crustal earthquakes like the 2001 Kokoxili earthquake are not expected to have significant non-double-couple components, the large non-double-couple components associated with the TW96

Model	Th.	Lat/Lon (°)	M_w	$\psi/\delta/\lambda$	ϵ (%)	m^2	BB
ICMT		35.84/92.45	7.83	97.5/90/0	–	–	
GCMT		35.80/92.91	7.78	94/61/-12	12	–	
S20RTS	GCA	35.88/92.77	7.92	98/40/0.86	5	0.17	
	FRT	35.92/92.80	7.81	97/55/-0.73	8	0.17	
vHW99	GCA	35.88/92.73	7.87	101/52/4.40	10	0.16	
	FRT	35.91/92.73	7.78	98/67/0.94	3	0.18	
TW95	GCA	35.98/92.55	7.89	99/46/1.41	3	0.17	
	FRT	36.00/92.52	7.79	99/59/2.23	5	0.19	
TW96	GCA	35.73/92.48	7.94	84/91/59.4	37	0.17	
	FRT	35.82/92.44	7.78	103/73/24.7	26	0.21	

Figure 4. Same as in Figure 2 but for the 2001 Kokoxili earthquake.

moment tensors indicate large uncertainties in the corresponding source mechanisms.

[21] The model of *Lasserre et al.* [2005] contains two distinct fault sections (Figure 5); a first section with a length of ~90 km at the western end of the rupture, along the Taiyang lake fault, and a second section about 400 km long, following the main Kunlun fault and the Kunlun Pass fault. The GCMT centroid epicenter (black circle in Figure 5) is about 42 km away from the ICMT epicenter (blue circle in Figure 5). Using the 3-D Earth models, the epicentral distance with respect to ICMT is reduced to about 29–33 km (FRT) for S20RTS, to 25–26 km for vHW99, to 18–19 km for TW95 and to 3–12 km for TW96. It is surprising that TW96 produces such good agreement with the ICMT centroid epicentral location, as it is the poorest fitting Earth model for this earthquake and, as discussed previously, it leads to a very uncertain focal mechanism.

[22] As an ad hoc experiment, we have also calculated a centroid from the InSAR model only taking into account the slip distribution in the second ~400 km long section of the fault system (red circle, which we denote ICMT2 location). We see that there is excellent agreement between this centroid location and the GCMT location, with a difference of about 2 km. Among the various solutions for the 3-D Earth models, the centroid location for the model S20RTS is now closer to the ICMT2 location (at distances of about 14 km and 11 km, for GCA and FRT modeling, respectively), followed by the solutions for the vHW99 model, which are at distances of about 18 km. TW96 is now the model with associated centroids the furthest away from the ICMT2 location (at distances of about 46 km and 50 km for GCA and FRT, respectively), which is consistent with the slightly larger misfits for this model and its lack of resolution for this earthquake. The solutions for TW95 are at distances of about 38 km and 42 km to the ICMT2 location. This sug-

gests that the differences between the ICMT location and the various locations obtained from seismic data may be at least partly due to uncertainties in the model of slip distribution of *Lasserre et al.* [2005]. A possible reason is that the InSAR data available for this study do not cover a few kilometers of the eastern end of the rupture, for which some large slip has been suggested [*Antolik et al.*, 2004; *Robinson et al.*, 2006]. Moreover, field measurements also show some slip beyond the eastern end of the InSAR slip model of *Lasserre et al.* [2005] [*Xu et al.*, 2006]. Another possibility is that there might be a slight overestimation of the slip in the first fault segment, as the associated standard deviation is relatively high [*Lasserre et al.*, 2005]. While the meaning of the spatial centroid is questionable for such a long rupture, here we use the estimated centroids essentially as tools to assess the quality of the slip model.

4. Results

[23] In this section we compare the various CMT parameters that we have obtained using the suite of 3-D Earth models and formulations considered with those in the ICMT archive compiled in paper 1. As for the GCMT technique, in our inversions sometimes the source became shallower than 15 km, so that in those cases it was fixed to be h = 15 km; thus in this paper we do not carry out comparisons for the source depth. Table 2 shows the average data misfit (m^2) over all the 32 studied earthquakes, using different Earth models and the two different theories (GCA and FRT):

$$m^2 = \frac{(\mathbf{s} - \mathbf{d})^T (\mathbf{s} - \mathbf{d})}{\mathbf{d}^T \mathbf{d}}, \tag{2}$$

where $\mathbf{d}$ is the data vector and $\mathbf{s}$ is the vector with the corresponding theoretical seismogram. We find results similar
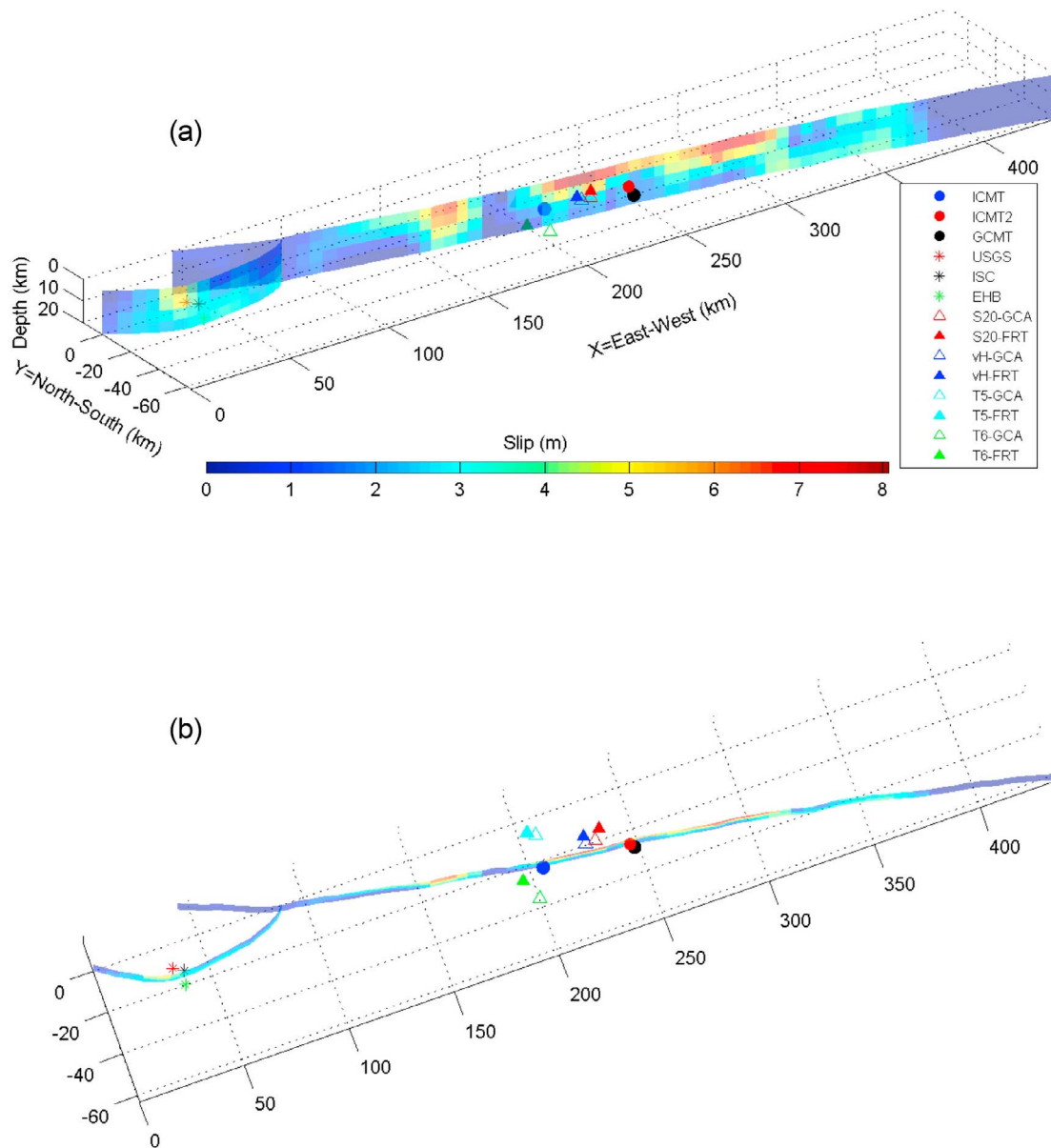
Figure 5. Comparison of centroid locations for the 2001 Kokoxili earthquake from various seismic catalogs (GCMT, USGS, ISC and EHB), from our inversions using a variety of Earth models and two different forward modeling strategies (S20-GCA, S20-FRT, vH-GCA, vH-FRT, T5-GCA, T5-FRT, T6-GCA and T6-FRT) and for the centroid calculated from the slip distribution obtained by *Lasserre et al.* [2005] using InSAR data (ICMT). (a) The distribution of slip in the model of *Lasserre et al.* [2005] superimposed on the various centroid locations. (b) A map view of the fault's surface projection and the various centroid locations (see text for more details).

to those in the analysis of the two earthquakes in section 3; overall, vHW99 and S20RTS produce slightly better fits to the data than TW95 and TW96, and for these two latter models, using the GCA leads to slightly improved data fits. Nevertheless, the differences in data fit are relatively small.

4.1. Moment Magnitude

[24] Figure 6a shows the moment magnitude values estimated for all the earthquakes investigated in this study for the various Earth models and theoretical formulations used.

The variability in moment magnitude due to Earth structure and/or to different theories is generally smaller than 0.2 for a given earthquake, with a median variability of 0.09. The greatest variability in moment magnitude as we change the Earth model used in the modeling is for the 2005, M_w 6.5 Fukuoka earthquake (earthquake 22), with a difference of 0.27 between the moment magnitude obtained using the Earth model S20RTS (which estimates $M_w = 6.50$ and $M_w = 6.57$ for FRT and GCA, respectively) and the Earth model TW95 (which estimates $M_w = 6.72$ and $M_w = 6.77$,

Table 2. Average of Misfit Values (equation (2)) for All the 32 Studied Earthquakes Using Different Earth Models and Theoretical Formulations[a]

	S20RTS	vHW99	TW95	TW96
GCA	0.18	0.18	0.21	0.20
FRT	0.18	0.18	0.22	0.23

[a]See Table 1 and text for more details.

respectively). As in previous cases, TW95 is the worst fitting model for this earthquake, so the corresponding moment magnitudes are probably quite uncertain. In some cases, the range of values of moment magnitude obtained from some of our inversions is closer to the ICMT moment magnitude than the GCMT magnitude (e.g., for earthquakes 9, 16, 22 and 23). However, in other cases, the reverse situation occurs (e.g., for earthquakes 17, 26, 29 and 32).

[25] Figure 7 shows the distribution of differences in moment magnitude between the various solutions found in this study and InSAR solutions. For reference, we also show the distribution of differences between ICMT and GCMT moment magnitudes for the earthquakes studied. As for the GCMT moment magnitude solutions, we find that in all cases the magnitudes determined using long-period seismic data are similar to those determined using InSAR data, with a slight tendency to estimate larger magnitudes than by InSAR. Using the FRT approach with the S20RTS model reduces the median of magnitude differences to half of that for the GCMT magnitudes; however, given the large standard deviations of all distributions, the significance of this result is unclear. Using the FRT with the model vHW99 leads to a distribution very similar to that for the GCMT, whereas TW95 and TW96 have the largest medians and standard deviations. It is interesting that for all models, using the great circle approximation leads to broader dis-
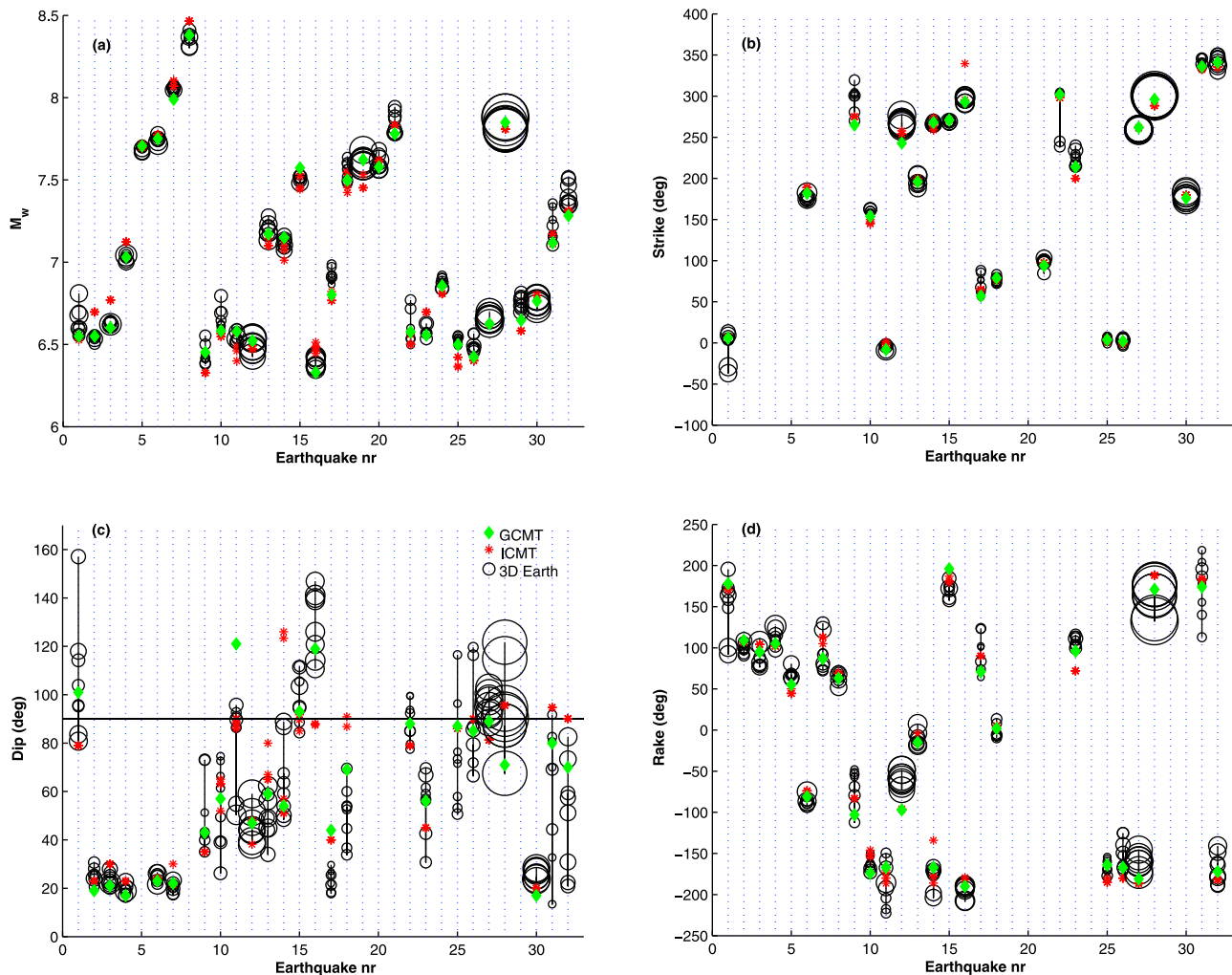

Figure 6. Comparison of (a) ICMT moment magnitude, M_w, (b) fault strike, (c) dip and (d) rake (red stars) with those determined in this study using the various Earth models and modeling strategies (black circles) for the 32 studied earthquakes (see Table 1 for key). The size of the black circles depends on the misfit value for that specific earthquake source model; the black circle in the legend ("3-D Earth") corresponds to a misfit of $m^2 = 0.16$ (see equation (2)). The GCMT parameters (green diamonds) are also shown for comparison. Fault dip values greater than 90° mean that the corresponding fault is dipping in the opposite direction to those with dip smaller than 90° for the same earthquake.
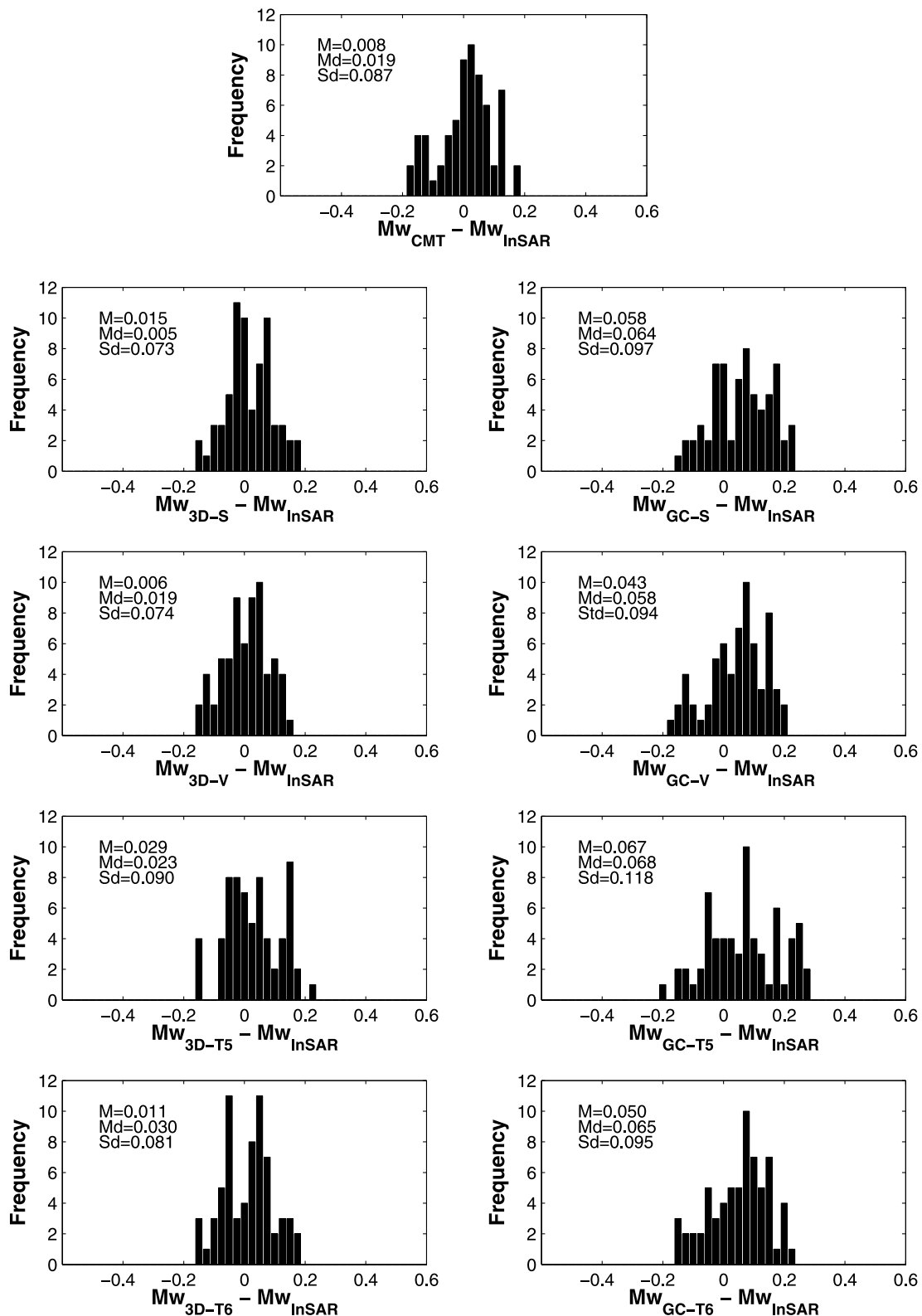
Figure 7. (top) Distribution of the difference between InSAR and GCMT moment magnitudes for the earthquakes used in this study. (bottom) Same as Figure 7 (top) but for the new seismic determinations using various Earth models and modeling strategies carried out in this study. A total of 66 points are plotted in all diagrams and the mean (M), median (Md) and standard deviation (Sd) are shown in the top corner of each plot. The 3D denotes a full ray theory calculation and GC denotes a great circle approximation calculation. S denotes the model S20RTS, V denotes the vHW99 model, T5 denotes the TW95 model, and T6 denotes the TW96 model.

tributions than those for the FRT approach and there is on average a greater disagreement with the ICMT magnitudes for GCA than for the FRT. Moreover, the apparent bias of seismic data producing larger magnitudes than InSAR is stronger when using the great circle approximation.

4.2. Fault Geometry and Mechanism

[26] Figure 6b shows the strike values estimated for all the earthquakes in this study, for the various Earth models and theoretical formulations used. There is little variability in strike due to different Earth models used and/or to different modeling strategies; the median variability is of 14°, with the maximum variability (66°) occurring for the 2005, M_w 6.5 Fukuoka earthquake (earthquake 22), due to the model TW95 predicting a too low strike value compared with the other models. In general, the strike values determined in our inversions are very similar to those in the GCMT catalog. Figure 8 shows the various distributions of differences between the strike values found in this study and those obtained using InSAR. We do not use strike, dip and rake values that were fixed in some InSAR studies (see paper 1). As in the comparisons between ICMT and GCMT parameters (see paper 1 and M = −1.621 diagram in Figure 8), there are large differences in strike (greater than 40°) for the 2004 Al Hoceima earthquake between all our solutions and the InSAR solution of *Tahayt et al.* [2009]. Other than that outlier, there is good agreement between the strike values found in our inversions and the ICMT strike values, with the models S20RTS and vHW99 showing the smallest differences, which are similar to those between the GCMT and ICMT solutions. TW95 has the largest medians of differences to ICMT values and standard deviations. As for the moment magnitude, using the GCA leads to larger differences in strike for the models S20RTS, vHW99 and TW96.

[27] Figure 6c shows the dip values estimated for all the earthquakes in this study, for the various Earth models and theoretical formulations used. In contrast with strike, there are large variations in the fault dip angles for a given earthquake when changing the Earth model or the modeling technique, with a median variability of about 32° and a maximum variability of 78° for the Hector Mine earthquake, due to the S20RTS (GCA) model predicting a very shallow-dipping solution (dip of 13.4°). Interestingly, for the subduction earthquakes studied here (earthquakes 3 to 7), all the results are very consistent between the various solutions. However, for some other earthquakes, there are solutions actually dipping in opposite directions for a given earthquake (e.g., for earthquakes 1, 15, 22, 25, 26 and 28). This great variability illustrates well the lack of robustness in fault dip determinations using long-period surface waves only and thus its great sensitivity to changes in Earth models, modeling strategies, etc. The distribution of differences between GCMT and ICMT dip values is narrower than for our solutions (see Figure 9). Nevertheless, even if slightly larger, the differences between S20RTS (FRT) and ICMT are similar to those for the GCMT dip values. As with the previous parameters, using TW95 leads to broader distributions and to larger differences in dip angle with respect to the ICMT values.

[28] Similar to the fault dip, there is also a large variability of rake values (see Figure 6d) for a given earthquake, with a median intraevent variability of about 30°. A maximum

variability in rake of 106° occurs for the Hector Mine earthquake, due to TW95 GCA giving a rake of 113° (compared with ICMT rake values of ~176°–185°). The distributions of differences in rake for the various solutions (Figure 10) show large standard deviations and all have median values well larger than the GCMT values (particularly for the TW95 model).

[29] As in paper 1, we do not find any relationship between differences in strike, dip and rake and other parameters such as moment magnitude, InSAR measurement period, non-double-couple component of the earthquakes reported in the global CMT catalog and earthquake depth.

4.3. Centroid Epicentral Location

[30] Figure 11 compares the distributions of epicentral distance between InSAR and seismic determinations using the various 3-D Earth models and theories. There is considerable variability in the shape of the various distributions as a function of the 3-D model used. All the distributions of differences in epicentral location for the various 3-D Earth models considered here have smaller standard deviations than the GCMT distribution, but their medians are generally larger than for GCMT, except for the model vHW99. Using this model leads to the smallest median of differences in epicentral distance of about 18 km, which is similar to the median of differences for the GCMT locations (16 km).

[31] For all the 3-D Earth models, there are large differences in epicentral location (greater than 40 km) for the 2001 M_w 6.8 Nisqually earthquake, which occurred within the subducting slab of the Juan de Fuca plate in the Cascadia subduction zone. In contrast, for the GCMT location there is a difference of 11.5 km compared to the InSAR epicentral location. A possible reason for these discrepancies is that the GCMT solution was obtained using more body wave records than surface waves; this suggests that inaccuracies in the Earth models that we use to model surface waves are causing the observed differences in epicentral location. Likewise, this might also explain the substantial differences in epicentral location between InSAR and our surface wave estimates for the 1992 M_w 7.3 Landers earthquake, with epicentral differences over 40 km for all the 3-D Earth models, notably when using the GCA. As noted for the GCMT locations in paper 1, for some subduction earthquakes in South America there are epicentral distances between InSAR and the various 3-D solutions greater than 40 km. This is particularly the case for the 1993 northern Chile earthquake (event 3 in Table 1) [*Pritchard et al.*, 2006], for all Earth models except for TW95, and for the 1995 Antofagasta earthquake (event 7 in Table 1) for TW96. Nevertheless, for the 1993, 1996 and 1998 Northern Chile earthquakes, most 3-D Earth models used lead to a better agreement with the InSAR locations compared to GCMT, with improvements of up to 40 km.

[32] Figure 12 shows the epicentral mislocation arrows relative to the InSAR solutions for the various Earth models. The mislocation arrows from inversions using the GCA and the FRT are very similar, so we show only arrows for the solutions using the FRT. The mislocation arrows for the models vHW99 and S20RTS show in general similar trends, such as earthquakes in South America being relocated toward the West of the ICMT location, which is also observed for the GCMT catalog. Mislocation arrows for earthquakes in Europe and in the Middle East are very consistent for these
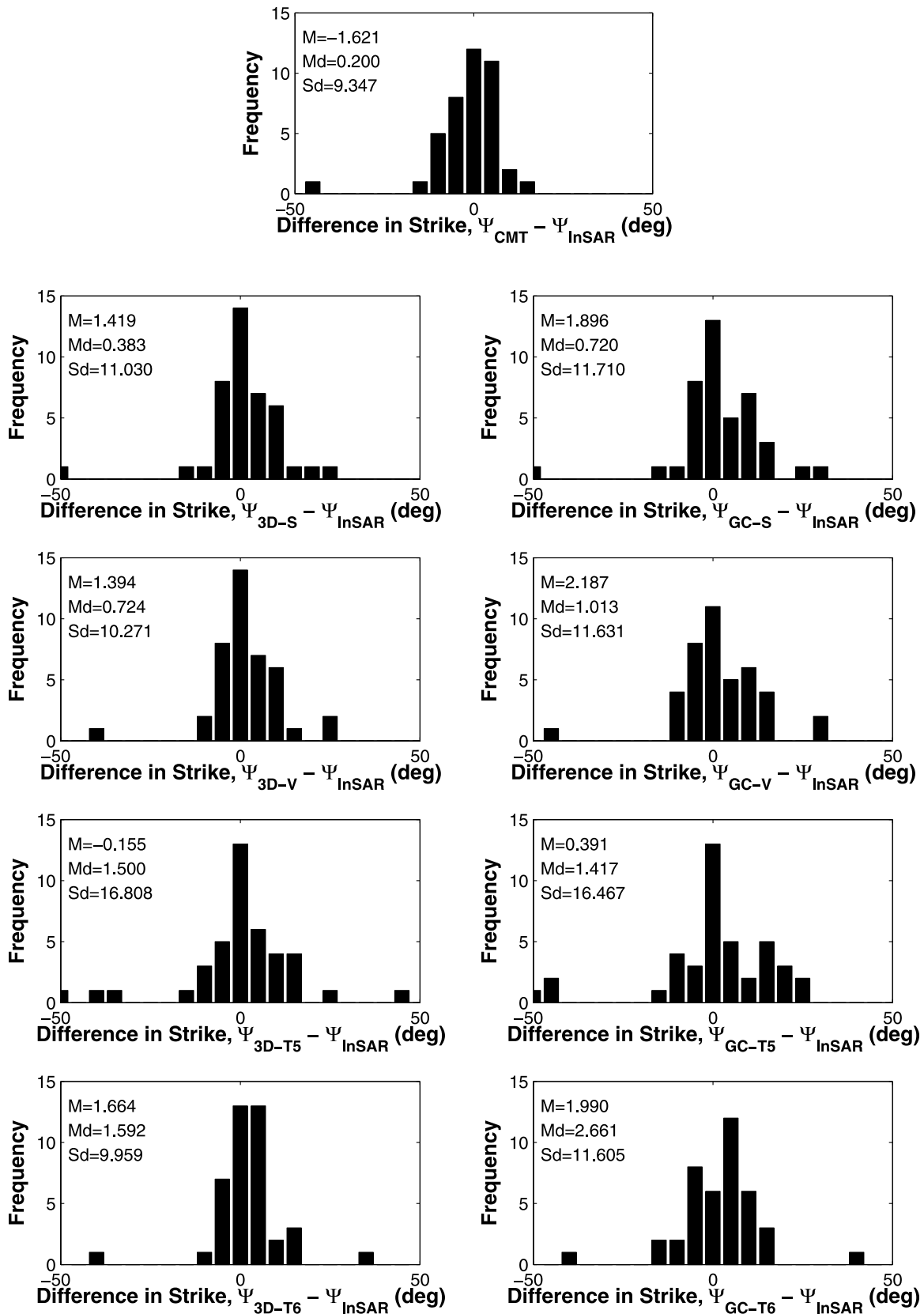
Figure 8. Same as in Figure 7 but for fault strike angle. A total of 40 points are plotted in all diagrams.
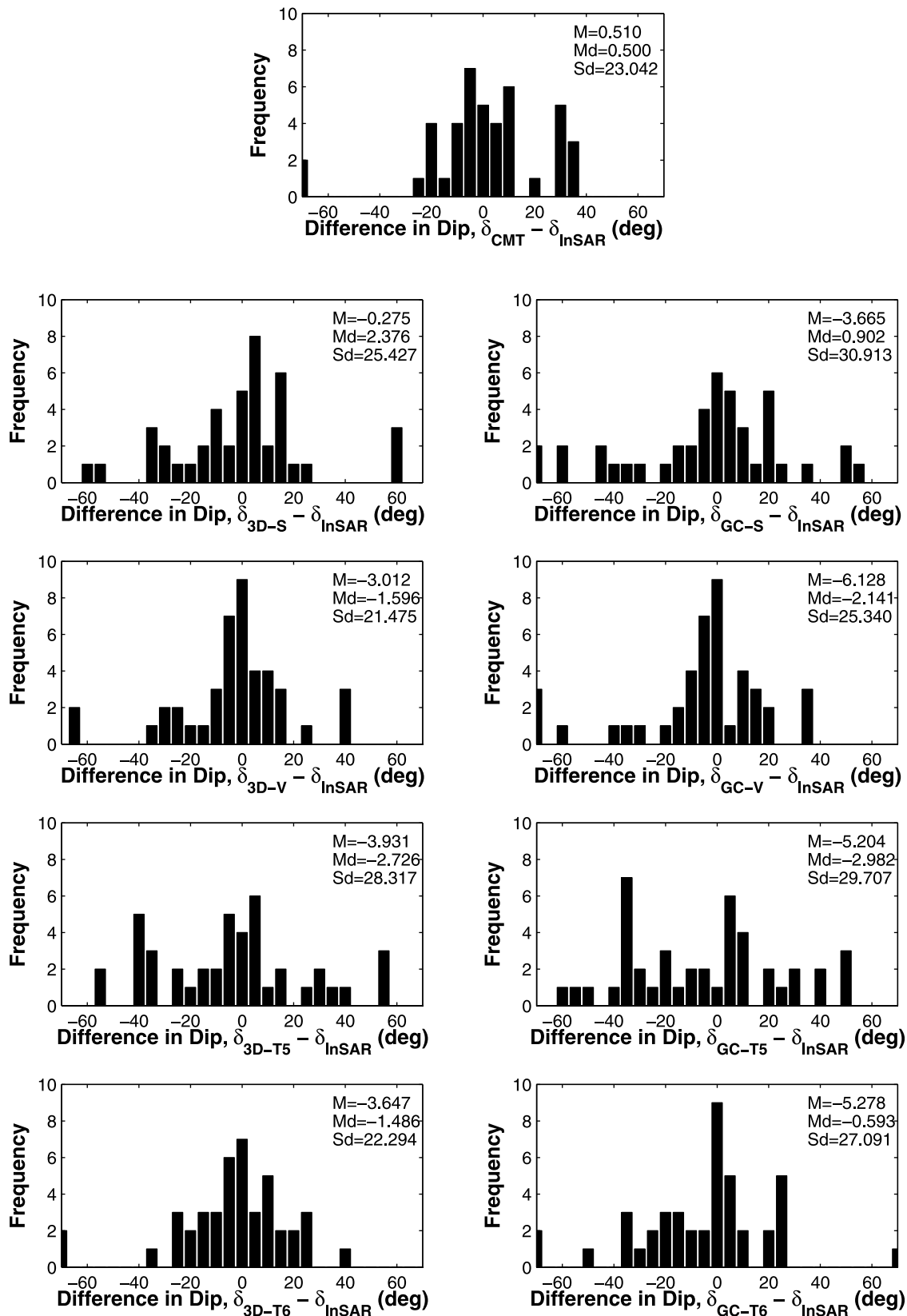
Figure 9. Same as in Figure 7 but for fault dip angle. A total of 43 points are plotted in all diagrams.
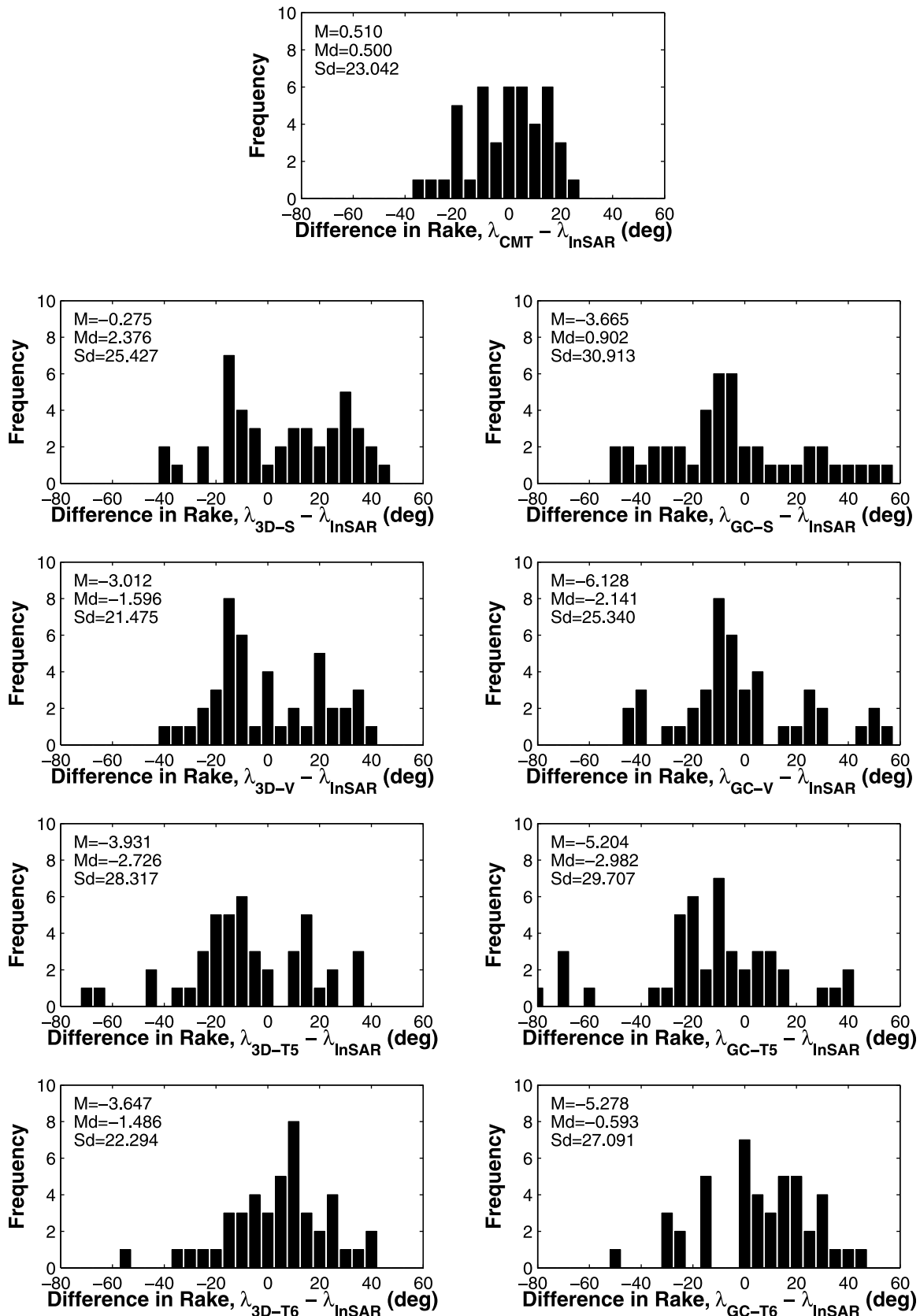
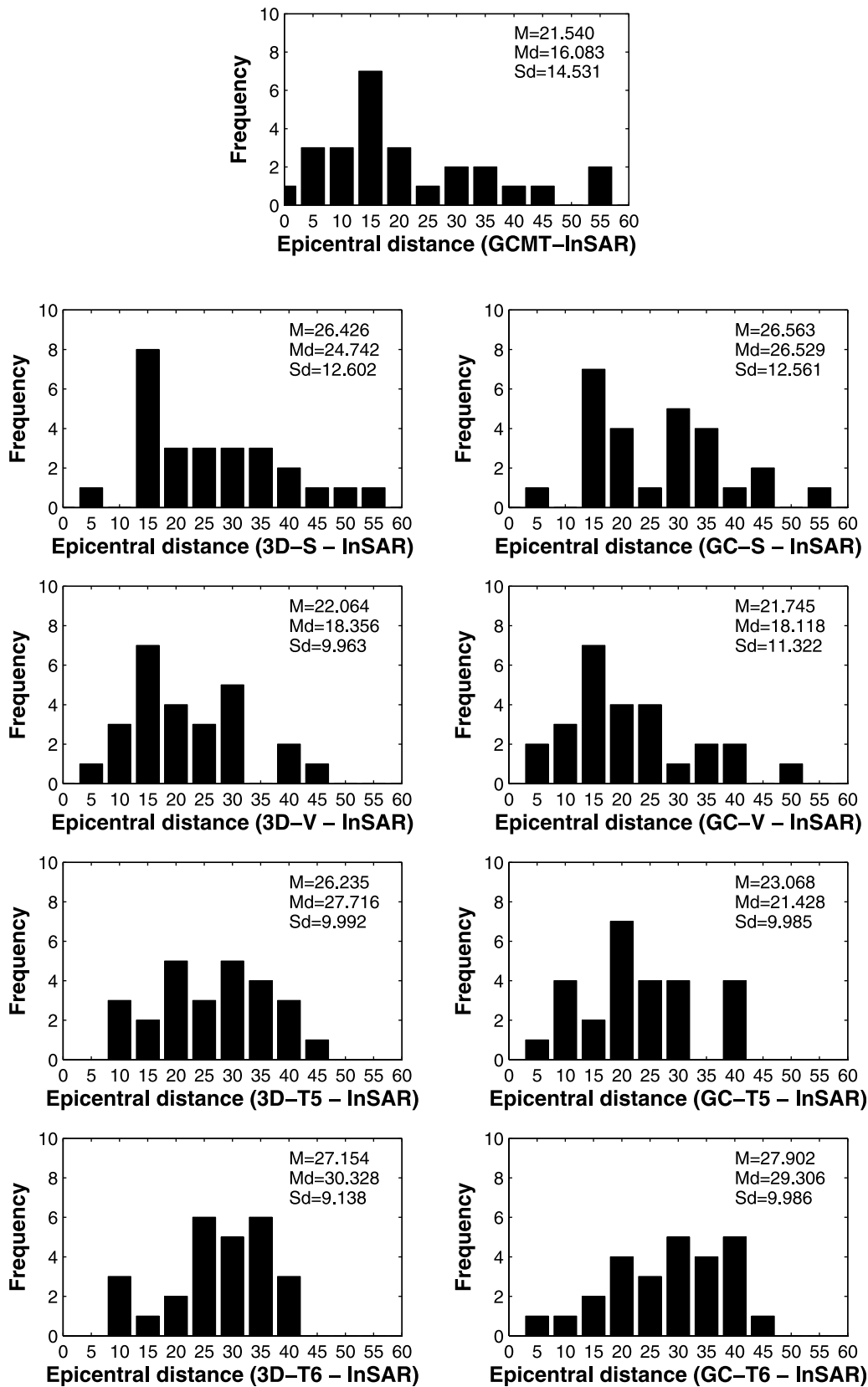**Figure 10.** Same as in Figure 7 but for fault rake angle. A total of 43 points are plotted in all diagrams.

Figure 11. Same as in Figure 7 but for differences in epicentral location. A total of 28 points are plotted in all diagrams.
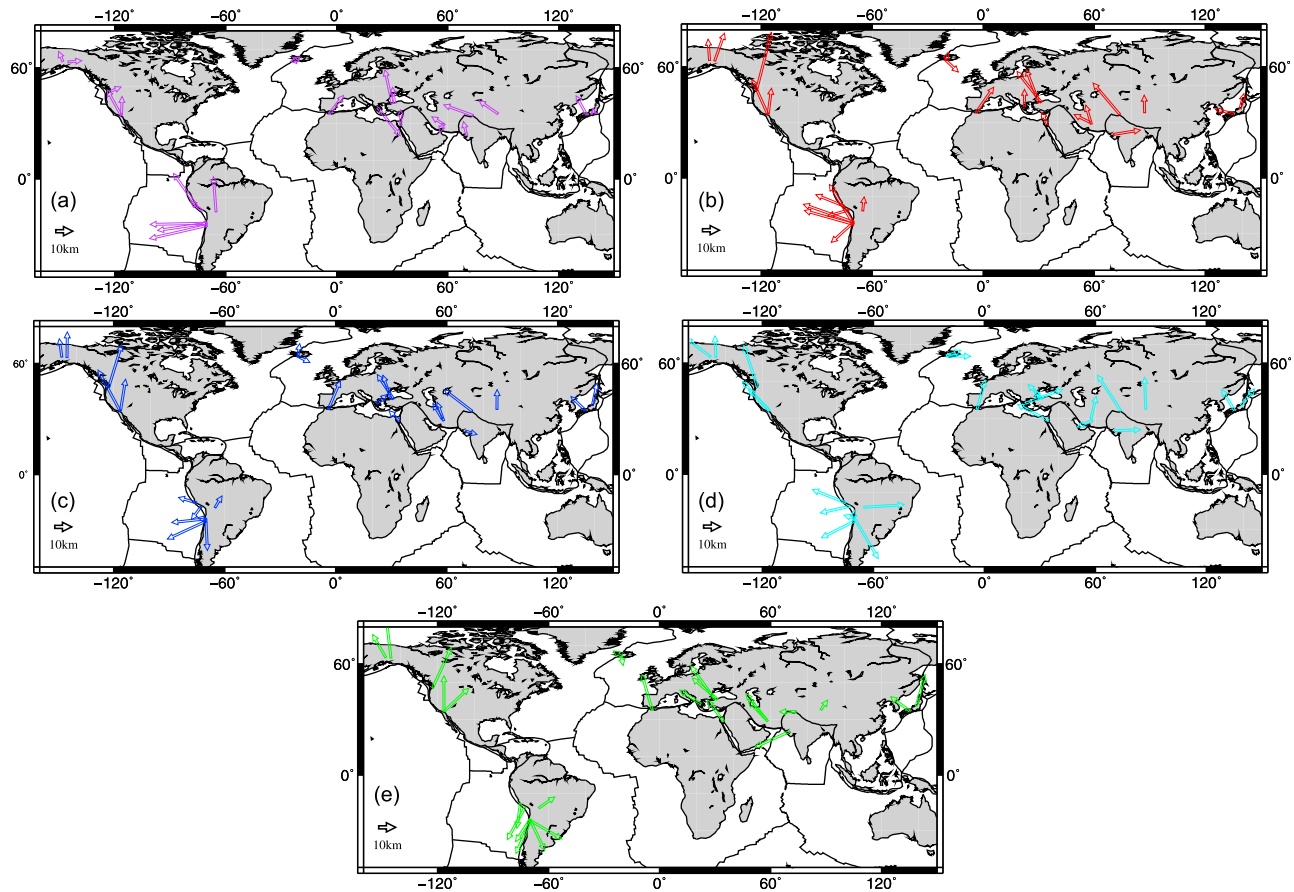
Figure 12. (a) Mislocation arrows between centroid epicentral locations determined using InSAR and those in the GCMT catalog (purple), as well as for the various 3-D Earth models used in this study, using (b) FRT, S20RTS (red), (c) vHW99 (blue), (d) TW95 (cyan) and (e) TW96 (green), for 28 earthquakes. The starting arrow point corresponds to the InSAR location. Note the arrow scale to the left in each diagram, which corresponds to 10 km.

two Earth models, with the seismic locations being generally toward the northwest compared to the ICMT locations. The model TW95 leads to somewhat different trends in the mislocation arrows, notably for earthquakes in South America, which show less geographic consistency than for the other models, thus suggesting less accurate locations. The same earthquakes are relocated toward the southwest when using the model TW96; nevertheless, this model leads to very consistent relocations toward the northwest in North Africa, Europe and Middle East.

[33] Similar to our findings in paper 1, we do not find any clear relationship between differences in centroid epicentral location and other parameters such as moment magnitude, InSAR measurement period, non-double-couple component of the earthquakes reported in the Global CMT catalog and earthquake depth.

5. Analysis of the Non-Double-Couple Component

[34] Earthquakes that cannot be modeled using a double-couple mechanism are inconsistent with shear failure on a single planar fault. For the earthquakes considered in this study, if a non-double-couple component is observed it may either be spurious or it may indicate shear rupture on a

nonplanar fault or on multiple fault planes with varying orientations. For shallow earthquakes, it is well known that the $M_{rr} - M_{\theta\theta}$ and $M_{r\theta} - M_{r\phi}$ components of the moment tensor, which are particularly sensitive to dip and rake, are difficult to constrain using long-period surface wave data only. Potentially, errors in these parameters may produce spurious deviations from a pure double-couple source mechanism. Thus, in this section we analyze the deviations from a pure double-couple (ϵ) in the source models that we obtain using the various 3-D Earth models and compare them with those in the GCMT catalog. Figure 13 shows the values of ϵ for the studied earthquakes. As expected, ϵ is small for the subduction earthquakes studied (earthquakes 2–8), which are all modeled by relatively simple planar fault models when using InSAR [se, e.g., *Pritchard et al.*, 2006]. Moreover, being large earthquakes, the seismic data have in general a high signal-to-noise ratio. For all the other earthquakes, there is a substantial variability in ϵ, which can be as much as 45%. For example, for the 1995 Kozani-Grevena earthquake (earthquake 12), all the 3-D models used lead to values of ϵ greater than 10%. Recent studies of this earthquake [e.g., *Rigo et al.*, 2004; *Resor et al.*, 2005] suggest that the rupture appears to have propagated across various fault segments with strike and dip changes of over 20°, which could explain the substantial non-double-couple
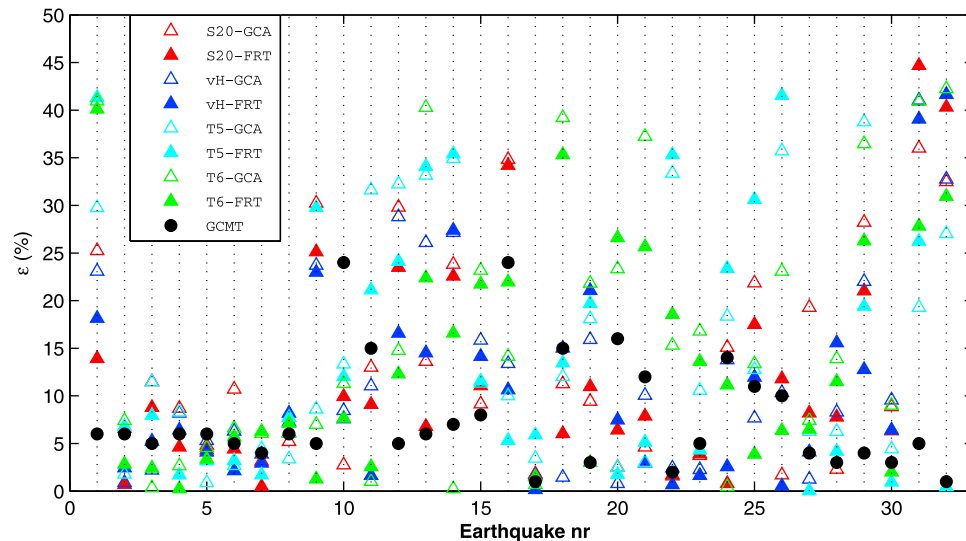
Figure 13. Deviations from a pure double-couple for the earthquake source parameters obtained using the various Earth models (triangles) and for GCMT solutions (black circles). Solid triangles correspond to solutions obtained using the FRT, whereas open triangles correspond to the GCA; ϵ quantifies the deviation from a pure double-couple mechanism, $\epsilon = |\lambda|_{min}/|\lambda|_{max}$, where λ are the eigenvalues of the seismic moment tensor.

components that we obtain using the various Earth models. Likewise, our 3-D Earth model inversions determine large values of ϵ for Landers (earthquake 32) and for Hector Mine (earthquake 31), for which various studies have suggested complex, multiple fault source mechanisms [e.g., *Fialko*, 2004; *Salichon et al.*, 2004; *Simons et al.*, 2002]. However, there are also some earthquakes with reported shear failure on a single planar fault for which using 3-D Earth models leads to large non-double-couple components. This is the case for example for Northridge (earthquake 29), which has been modeled in various studies using single-fault plane models with relatively simple slip patterns [e.g., *Hudnut et al.*, 1996; *Hartzell et al.*, 1996], for which we obtain non-double-couple components between 12% and 40%. As discussed in the next session, most likely these non-double-couple components are spurious.

[35] On average, the solutions that we obtain have larger deviations from a pure double-couple mechanism than the solutions from the GCMT catalog (Figure 14). However, it is interesting that for the models with poorer fit to the data (TW95 and TW96), ϵ is on average larger than for the other models, suggesting that using more accurate Earth models reduce artificial deviations from a pure double-couple mechanism. Moreover, using the great circle approximation also produces systematically larger average values of ϵ than the FRT, which indicates that using more accurate forward modeling methods helps reduce spurious non-double-couple components.

6. Discussion

[36] We have compared a range of earthquake source parameters determined using various Earth models and two different forward modeling strategies (GCA and FRT) with those determined using InSAR. As it was found by *Ferreira and Woodhouse* [2006], vHW99 and S20RTS lead to the best data fit and the FRT explains the data as well as the GCA, except for TW95 and TW96. Nevertheless, the differences in data fit are relatively small. Comparing the various centroid locations determined in this study for the M_w 6.6, 1998 Aiquile, Bolivia earthquake with that from the InSAR model of *Funning et al.* [2005] we find that using the Earth models vHW99, S20RTS and TW96 leads to epicentral locations about 11–17 km away from the ICMT location, which is consistent with the observed damage distribution for that event. This is a considerable improvement over the GCMT, ISC, EHB, USGS and TW95 locations, which are over 30 km away from the ICMT location, due to the use of inaccurate Earth structure. The comparison of the various centroid locations determined in this study for the M_w 7.8, 2001 Kokoxili earthquake with that for the variable slip model of *Lasserre et al.* [2005] allowed us to identify limitations in the slip distribution of this InSAR model and to better understand the intraevent variability of rupture models for this earthquake. This shows that carrying out seismic source inversions using a variety of Earth models and theories and comparing the solutions obtained with other independent source models taking the data fit into account is a valuable tool to assess epistemic uncertainties in the models.

[37] The median variability of moment magnitude for a given earthquake due to different Earth models and theories used in our source inversions is of about 0.1, thus being similar to the errors we might expect when comparing GCMT and ICMT magnitudes (see paper 1). The best fitting models (S20RTS and vHW99) produce smaller discrepancies between moment magnitudes determined using InSAR and seismic data than the other Earth models, with a median of differences of about 0.005–0.02 and a spread around 0.07. Thus, our comparisons with InSAR solutions indicate that, despite being small, the differences in misfit between the Earth models used are significant, with S20RTS and vHW99
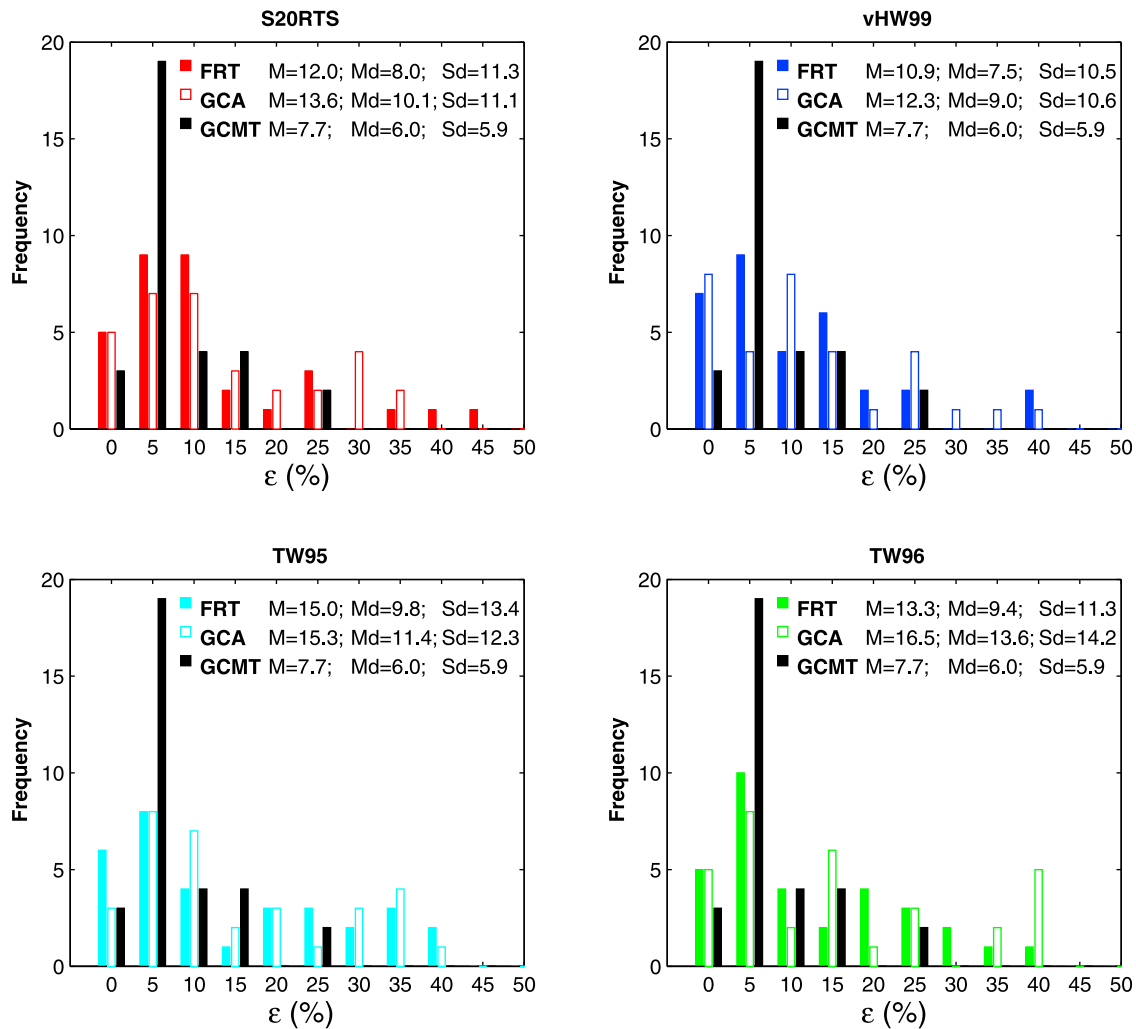
Figure 14. Distributions of the non-double-couple deviation parameter ϵ for the various Earth models and forward modeling techniques used in this study, as well as for the GCMT source parameters. The mean (M), median (Md) and standard deviation (Sd) of each distribution are also shown.

being overall the best quality models. Moreover, we show that compared to the FRT, the GCA leads to double or even larger discrepancies in seismic moment to the InSAR solutions and to a stronger bias of seismic data predicting larger seismic moments than InSAR. This is probably because whereas the GCA calculates surface wave amplitudes in a 1-D Earth model, the FRT is more accurate, as it calculates the amplitudes in the laterally varying Earth, taking focusing and defocusing effects into account. This improved modeling thus seems to reduce errors in estimated moment magnitudes, which depend linearly on the wave's amplitudes. *Ferreira and Woodhouse* [2006] also noticed a similar tendency when comparing the seismic moment determined using the GCA with that in the GCMT catalog for another set of large, shallow earthquakes. However, the absence of independent benchmark solutions together with small differences in data misfit with unclear significance prevented them from interpreting the observed tendency in detail. Since the ICMT magnitudes are determined in a different, independent way to seismic solutions, this study gives us for the first time a truly independent confirmation that using long-period surface waves only to model earthquakes combined with the GCA can lead to an overestimation of the seismic moment, particularly for the Earth models fitting the data less well. In addition, in this study we find similar trends for fault strike, which, as discussed in paper 1, is well determined using both InSAR and long-period seismic data.

[38] Our comparisons of fault dip angle show clearly the lack of resolution of long-period surface waves in estimating this parameter, with an intraevent variability of fault dip associated with the use of different Earth models and theories of about 32°. The distributions of differences in dip obtained in this study all have larger medians than when comparing ICMT and GCMT dip values, which is probably due to the fact that for some of these earthquakes GCMT used both surface and body waves, and the latter should have a better dip resolution. Nevertheless, the differences between S20RTS (FRT) and ICMT are smaller than for models with a poorer data fit. Thus, this study provides us with an objective, independent confirmation that despite intrinsic difficulties in inferring the dip fault angle using long-period

surface wave data, this problem somewhat reduces if we take lateral heterogeneity correctly into account.

[39] An equally large intraevent variability was found for fault rake angle, with this parameter showing the largest discrepancies to the ICMT solutions, well larger than when compared with GCMT values. This might be due to the fact that many of the earthquakes used in this study have near-vertical strike-slip mechanisms, whose dip and rake are particularly difficult to constrain using long-period surface wave data due to their insensitivity to the dip-slip components of the moment tensor. Synthetic tests by *Ferreira and Woodhouse* [2006] showed that for this type of faulting, errors in rake due to inaccurate Earth structure can be as much as 70° and larger than errors in dip angle, which is compatible with our findings.

[40] There are considerable differences between the InSAR epicentral locations and those obtained using the various 3-D Earth models. Since InSAR data have a fine spatial resolution and accuracy, these comparisons give us the opportunity to quantitatively assess the ability of the various Earth models and of long-period surface wave data to locate earthquakes. Despite all the distributions of differences in epicentral location for the 3-D models having smaller standard deviations than the GCMT distribution, their medians are generally larger than for GCMT, except for the model vHW99. The models TW95 and TW96 lead to the distributions of differences to ICMT locations with shapes differing the most from the GCMT distribution, with slightly higher median values and showing the least geographical consistency, particularly in South America. This suggests less accurate locations by these models. While for most subduction earthquakes in South America the 3-D Earth models lead to locations closer to the InSAR locations than those in the GCMT catalog, the opposite occurs for some earthquakes in North America. This is probably due to the fact that for some of these earthquakes the GCMT method uses body waves in addition to long-period surface waves. Indeed, *Hjörleifsdóttir and Ekström* [2010] showed that errors in epicentral location due to inaccurate 3-D Earth structure are reduced when combining different data types. In the same study, the authors used synthetic tests to estimate errors in GCMT parameters due to unmodeled structural heterogeneity. They calculated synthetic data using the Spectral Element Method for the mantle models S20RTS and S362ANI [*Kustowski et al.*, 2008] combined with CRUST2.0, which were inverted for earthquake source parameters using the standard Global CMT procedure. They found average errors in centroid location of about 10 km due to differences between the degree 8, SH8/U4L8 [*Dziewonski and Woodward*, 1992] Earth model used in the GCMT method and those used to generate the synthetic data. The errors that they found are much smaller than the differences in epicentral location that we find in this study for real earthquakes. As explained previously, part of the location differences that we obtain might be due to the fact that we use long-period surface waves only. However, contrasting our results with those of *Hjörleifsdóttir and Ekström* [2010] suggests that the observed differences are also due to the fact that the Earth models used in both studies are smooth; thus, at least part of the differences in epicentral locations that we find are probably due to the effects of small scale heterogeneity, which is not yet resolved by current global tomographic

models. This is further supported by the fact that the Earth model used in this study that leads to locations on average closer to InSAR locations is the vHW99 model, which contains the greatest amount of small scale heterogeneity and that has been shown to fit surface wave data very well in previous studies [*Ferreira and Woodhouse*, 2006, 2007b]. In addition to small scale heterogeneity, there are other aspects of the real Earth that are not represented in the four Earth models considered and that may also affect our results, such as for example anisotropy.

[41] With the exception of the South American subduction earthquakes used in this study, we often find substantial non-double-couple components in the solutions obtained using the various Earth models. While for some earthquakes the deviations from a pure double-couple obtained might be real and due to complex, multiple fault rupture mechanisms, for other earthquakes, they seem to be spurious. On average, the solutions obtained using the various 3-D Earth models have larger non-double-couple components than the GCMT solutions, which is possibly due to the fact that we only use long-period surface waves in our inversions, whereas for many earthquakes in this study the GCMT method uses both body and surface waves. Indeed, *Bukchin et al.* [2010] showed that multiple double-couple mechanisms can be obtained in CMT inversions of long-period surface wave data for shallow earthquakes. *Henry et al.* [2002] suggested a method for finding the optimal pure double-couple solution, which can be different from the best double-couple, and highlighted how spurious non-double-couple components can be especially problematic for strike-slip earthquakes. In the future it will be interesting to compare our pure double-couple solutions with results obtained using the method of *Henry et al.* [2002]. In addition, *Hjörleifsdóttir and Ekström* [2010] showed that errors in non-double-couple components can be reduced when using more than one wave type of data. The Earth models with poorer fit to the data (TW95 and TW96) and the great circle approximation lead to non-double-couple components on average larger than for the other models and for the full ray theory. This shows that the use of more accurate Earth models and forward modeling techniques reduce artificial deviations from a pure double-couple mechanism.

7. Conclusions

[42] In this study we compare CMT earthquake source parameters determined using InSAR with those obtained from seismic inversions of long-period surface wave data using four different Earth models and two different wave propagation theories for 32 large shallow continental earthquakes. We find that these comparisons are valuable to identify inaccuracies in the slip distribution models obtained using InSAR data. Conversely, the comparisons enable us to assess in a novel, truly independent way the effect of using incomplete theories and of unmodeled structural heterogeneity on long-period source parameter determinations, and to quantitatively compare different Earth models. We show that using the GCA biases moment magnitude determinations to larger magnitudes than those obtained using InSAR by a factor of more than two, compared to the FRT. Moreover, this bias is also reduced by about a factor of two when using the best fitting Earth models (S20RTS and vHW99). Thus,

despite being small, the differences in overall data misfit between the best (S20RTS and vHW99) and poorest (TW95 and TW96) fitting Earth models are significant, with S20RTS and vHW99 being overall the best quality models. Likewise, using the FRT together with the models S20RTS and vHW99 leads to smaller median differences in fault strike angle compared to the InSAR determinations by factors up to two. As expected for long-period surface wave source inversions for shallow earthquakes, fault dip and rake angles are difficult to constrain, but this problem is reduced when using the best fitting Earth models, notably vHW99 combined with FRT. We identify some substantial non-double-couple components for some earthquakes that might be real and associated with complex, multiple fault rupture mechanisms. However, we also show that artificial non-double-couple components are on average larger for the Earth models with poorer fit to the data and for the less accurate GCA. There are substantial differences between InSAR epicentral locations and those obtained in this study using the various Earth models, with median differences ranging from 18 to 30 km. On average, no clear improvements to the GCMT locations are obtained, suggesting that more detailed, higher-resolution Earth models are necessary to further refine CMT epicentral locations. This issue deserves further future investigation.

References

Antolik, M., R. E. Abercrombie, and G. Ekström (2004), The 14 November 2001 Kokoxili (Kunlunshan), Tibet, earthquake: Rupture transfer through a large extensional step-over, *Bull. Seismol. Soc. Am.*, *94*(4), 1173–1194, doi:10.1785/012003180.

Bassin, C., G. Laske, and G. Masters (2000), The current limits of resolution for surface wave tomography in North America, *Eos Trans. AGU*, *81*(52), F897.

Bernardi, F., J. Braunmiller, U. Kradolfer, and D. Giardini (2004), Automatic regional moment tensor inversion in the European-Mediterranean region, *Geophys. J. Int.*, *156*, 1–14.

Bukchin, B., E. Clévédé, and A. Mostinskiy (2010), Uncertainty of moment tensor determination from surface wave analysis for shallow earthquakes, *J. Seismol.*, *14*, 601–614, doi:10.1007/s10950-009-9185-8.

Dziewonski, A. M., and J. H. Woodhouse (1983), Studies of the seismic source using normal-mode theory, *Proc. Enrico Fermi Int. Sch. Phys.*, *LXXXV*, 45–137.

Dziewonski, A. M., and R. L. Woodward (1992), Acoustic imaging at the planetary scale, in *Acoustical Imaging 19*, pp. 785–797, Plenum, New York.

Dziewonski, A. M., T.-A. Chou, and J. H. Woodhouse (1981), Determination of earthquake source parameters from waveform data for studies of global and regional seismicity, *J. Geophys. Res.*, *86*, 2825–2852, doi:10.1029/JB086iB04p02825.

Ferreira, A. M. G., and J. Woodhouse (2006), Long period seismic source inversions using global tomographic models, *Geophys. J. Int.*, *166*(3), 1178–1192, doi:10.1111/j.1365-246X.2006.03003.x.

Ferreira, A. M. G., and J. Woodhouse (2007a), Source, path and receiver effects on seismic surface waves, *Geophys. J. Int.*, *168*, 109–132, doi:10.1111/j.1365-246X.2006.03092.x.

Ferreira, A. M. G., and J. Woodhouse (2007b), Observations of long period Rayleigh wave ellipticity, *Geophys. J. Int.*, *169*, 161–169, doi:10.1111/j.1365-246X.2006.03276.x.

Fialko, Y. (2004), Probing the mechanical properties of seismically active crust with space geodesy: Study of the coseismic deformation due to the 1992 M_w 7.3 Landers (southern California) earthquake, *J. Geophys. Res.*, *109*, B03307, doi:10.1029/2003JB002756.

Funning, G. J., R. M. D. Barker, S. H. Lamb, E. Minaya, B. Parsons, and T. J. Wright (2005), The 1998 Aiquile, Bolivia earthquake: A seismically active fault revealed with InSAR, *Earth Planet. Sci. Lett.*, *232*, 39–49, doi:10.1016/j.epsl.2005.01.013.

Hartzell, S., P. Liu, and C. Mendoza (1996), The 1994 Northridge, California, earthquake: Investigation of rupture velocity, risetime, and high-frequency radiation, *J. Geophys. Res.*, *101*(B9), 20,091–20,108, doi:10.1029/96JB01883.

Henry, C., J. H. Woodhouse, and S. Das (2002), Stability of earthquake moment tensor inversions: effect of the double-couple constraint, *Tectonophysics*, *356*, 115–124, doi:10.1016/S0040-1951(02)00379-7.

Hjörleifsdóttir, V., and G. Ekström (2010), Effects of three-dimensional Earth structure on CMT earthquake parameters, *Phys. Earth Planet. Inter.*, *179*, 178–190, doi:10.1016/j.pepi.2009.11.003.

Hudnut, K. W., et al. (1996), Coseismic displacements of the 1994 Northridge, California earthquake, *Bull. Seismol. Soc. Am.*, *86*(1), S19–S36.

Kustowski, B., G. Ekström, and A. M. Dziewonski (2008), Anisotropic shear-wave velocity structure of the earth's mantle: A global model, *J. Geophys. Res.*, *113*, B06306, doi:10.1029/2007JB005169.

Lasserre, C., G. Peltzer, F. Crampé, Y. Klinger, J. Van der Woerd, and P. Tapponnier (2005), Coseismic deformation of the 2001 M_w = 7.8 Kokoxili earthquake in Tibet, measured by synthetic aperture radar interferometry, *J. Geophys. Res.*, *110*, B12408, doi:10.1029/2004JB003500.

Patton, H. J., and G. E. Randall (2002), On the causes of biased estimates of seismic moment for earthquakes in central Asia, *J. Geophys. Res.*, *107*(B11), 2302, doi:10.1029/2001JB000351.

Pondrelli, S., A. Morelli, G. Ekström, S. Mazza, E. Boschi, and A. M. Dziewonski (2002), European-Mediterranean regional centroid moment tensors catalog: 1997–2000, *Phys. Earth Planet. Inter.*, *130*, 71–101, doi:10.1016/S0031-9201(01)00312-0.

Pritchard, M. E., C. Ji, and M. Simons (2006), Distribution of slip from 11 $M_w \geq 6$ earthquakes in the northern Chile subduction zone, *J. Geophys. Res.*, *111*, B10302, doi:10.1029/2005JB004013.

Resor, P. G., D. D. Pollard, T. J. Wright, and G. C. Beroza (2005), Integrating high-precision aftershock locations and geodetic observations to model coseismic deformation associated with the 1995 Kozani-Grevena earthquake, Greece, *J. Geophys. Res.*, *110*, B09402, doi:10.1029/2004JB003263.

Rigo, A., J.-B. de Chabalier, B. Meyer, and R. Armijo (2004), The 1995 Kozani-Grevena (northern Greece) earthquake revisited: An improved faulting model from synthetic radar interferometry, *Geophys. J. Int.*, *157*, 727–736, doi:10.1111/j.1365-246X.2004.02220.x.

Ritsema, J., H. van Heijst, and J. Woodhouse (1999), Complex shear wave velocity structure imaged beneath Africa and Iceland, *Science*, *286*, 1925–1928, doi:10.1126/science.286.5446.1925.

Robinson, D. P., C. Brough, and S. Das (2006), The M_w 7.8, 2001 Kunlunshan earthquake: Extreme rupture speed variability and effect of fault geometry, *J. Geophys. Res.*, *111*, B08303, doi:10.1029/2005JB004137.

Salichon, J., P. Lundgren, B. Delouis, and D. Giardini (2004), Slip history of the 16 October 999 M_w 7.1 Hector Mine earthquake (California) from the inversion of InSAR, GPS, and eleseismic data, *Bull. Seismol. Soc. Am.*, *94*, 2015–2027, doi:10.1785/0120030038.

Simons, M., Y. Fialko, and L. Rivera (2002), Coseismic deformation from the 1999 M_w 7.1 Hector Mine, California, earthquake as inferred from InSAR and GPS observations, *Bull. Seismol. Soc. Am.*, *92*, 1390–1402, doi:10.1785/0120000933.

Tahayt, A., et al. (2009), The Al Hoceima (Morocco) earthquake of 24 February 2004, analysis and interpretation of data from ENVISAT ASAR and SPOT5 validated by ground-based observations, *Remote Sens. Environ.*, *113*, 306–316, doi:10.1016/j.rse.2008.09.015.

Trampert, J., and J. H. Woodhouse (1995), Global phase-velocity maps of Love and Rayleigh-waves between 40 and 150 seconds, *Geophys. J. Int.*, *122*, 675–690, doi:10.1111/j.1365-246X.1995.tb07019.x.

Trampert, J., and J. H. Woodhouse (1996), High resolution global phase velocity distributions, *Geophys. Res. Lett.*, *23*, 21–24, doi:10.1029/95GL03391.

van Heijst, H. J., and J. H. Woodhouse (1999), Global high-resolution phase velocity distributions of overtone and fundamental-mode surface waves determined by mode branch stripping, *Geophys. J. Int.*, *137*, 601–620, doi:10.1046/j.1365-246x.1999.00825.x.

Weston, J., A. Ferreira, and G. Funning (2011), Global compilation of interferometric synthetic aperture source models: 1. Comparisons with seismic catalogues, *J. Geophys. Res.*, doi:10.1029/2010JB008131, in press.

Woodhouse, J. H., and A. M. Dziewonski (1984), Mapping the upper mantle: Three-dimensional modeling of Earth structure by inversion of waveforms, *J. Geophys. Res.*, *89*, 5953–5986, doi:10.1029/JB089iB07p05953.

Xu, X., G. Yu, Y. Klinger, P. Tapponnier, and J. Van Der Woerd (2006), Reevaluation of surface rupture parameters and faulting segmentation of the 2001 Kunlunshan earthquake (M_w 7.8), northern Tibetan Plateau, China, *J. Geophys. Res.*, *111*, B05316, doi:10.1029/2004JB003488.

A. M. G. Ferreira and J. Weston, School of Environmental Sciences, University of East Anglia, Norwich NR4 7TJ, UK. (A.Ferreira@uea.ac.uk; J.Weston@uea.ac.uk)

G. J. Funning, Department of Earth Sciences, University of California, Riverside, CA 92521, USA. (gareth@ucr.edu)